Spring 7-1-2017

Manipulating the Optical Properties of Hollow Pd/Ag and Pt/Ag Nanoparticles Synthesized by Galvanic Replacement Reaction

Salvador Alcantar
Governors State University

Manipulating the Optical Properties of Hollow Pd/Ag and Pt/Ag Nanoparticles Synthesized by Galvanic Replacement Reaction

A Project Submitted to:

Governors State University

By: Salvador Alcantar

In partial fulfillment of the requirement for the Masters of Analytical Chemistry

May 2017

Governors State University

University Park, Illinois

This paper is dedicated to my professors, parents, family, friends, and to all of those who supported me through my academic journey.

Acknowledgements

My most heartfelt thanks to Dr. Ranmohotti for the support, resources, time, assistance, and mentoring he provided in order to help me complete this research project. I would also like to thank Dr. Shin, Dr. Henne, and Dr. Kumar for their assistance and direction during my undergraduate and graduate work. I also thank our collaborator for transmission electron microscopy images.

I would like to express my gratitude to other members of the Chemistry Department for their assistance during my time here at Governors State University including Catherine Toffora, Janith Wazio, Dr. Sowa, and all the professors I was fortunate enough to assist as a graduate assistant. Finally, I would like to thank Joseph Zuklic, Vincent Schmitz, and Michael Villanueva for putting up with me over the last three years. I would not have been able to make it through this program without the three of you.

Table of Contents

List of Figures

metal takes place on the surface of the template to form a shell while the first metal is continuously consumed from the core.

Figure 3. Schematic illustration of the morphological and structural evaluations at different stages of the galvanic replacement reaction between Ag nanoprism and $HAuCl_4$ in an aqueous solution.

Figure 4. Programmable syringe pump used to gradually add small amounts of solution of $AgNO_3$ and $HAuCl_4$ at a given rate.

Table 1. Volumes of seed solution used to prepare silver nanoprisms with different sizes and their SPR peak position.

Figure 5. UV-Visible absorption spectra of the series of Ag nanoprisms obtained by using different volumes of seed solution: 650 μL, 120 μL, 120 μL, and 20 μL.

Figure 6. Photograph of the series of Ag nanoprism samples illustrating the range of colors obtained using different volumes of seed solutions: 20 μL, 120 μL, 200 μL, and 650 μL.

Figure 7. UV-Visible absorption spectra of the series of Pd/Ag samples obtained by addition of 40 μL, 80 μL, 120 μL, 160 μL, 200 μL, 240 μL, 280 μL, 320 μL, 360 μL, and 400 μL of K_2PdCl_4 (0.5 mM) in the presence of ascorbic acid to the Ag nanoprisms prepared by using of 120 μL of silver seed solution.

Figure 8. Photograph of the Ag nanoprism solution obtained by using 120 μL of seed solution (left) and Pd/Ag samples obtained by addition of 400 μL of K_2PdCl_4 solution (right).

Figure 9. UV-Visible absorption spectra of the series of Pt/Ag samples obtained by addition of 40 μL, 80 μL, 120 μL, 160 μL, 200 μL, 240 μL, 280 μL, 320 μL, 360 μL, and 400 μL of K_2PdCl_4 (0.5 mM) in the presence of ascorbic acid to the Ag nanoprisms prepared by using of 120 μL of silver seed solution.

Figure 10. Photograph of Ag nanoprism solution obtained by using 120 μL of seed solution (left) and Pt/Ag samples obtained by addition of 400 μL of K_2PtCl_4 solution (right).

Figure 11. UV-Visible absorption spectra of the series of Au/Ag samples obtained by addition of 2 mL, 4 mL, 6 mL, 8 mL, 10 mL, 15 mL, 20 mL, 30 mL, 40 mL, 50 mL, and 60 mL of HAuCl4 (0.5 mM) in the presence of ascorbic acid to the Ag nanoprisms prepared by using of 120 μL of silver seed solution.

Figure 12. UV-Visible absorption spectra of the series of Pd/Ag samples obtained by addition of 10 mL, 20 mL, 30 mL, 40 mL, 50 mL, and 60 mL of K_2PdCl_4 (0.5 mM) in the presence of ascorbic acid to the Ag nanoprisms prepared by using of 120 μL of silver seed solution.

Figure 13. UV-Visible absorption spectra of the series of Pt/Ag samples obtained by addition of 2 mL, 4 mL, 6 mL, 8 mL, 10 mL, 20 mL, 30 mL, 40 mL, 50 mL, and 60 mL of K_2PtCl_4 (0.5 mM) in the presence of ascorbic acid to the Ag nanoprisms prepared by using of 120 μL of silver seed solution.

Figure 14. TEM images of the individual (A) Au/Ag, (B) Pd/Ag, and (C) Pt/Ag nanoshells. The dark contrast areas in A and B represent the multilayers of nanoshells showing the 3-dimensional connectivity of nanoscale.

Abstract

Considerable efforts have recently been devoted to the fabrication of metallic nanostructures on account of their tunable morphologies which can lead to new and fascinating optical properties. These properties of a metallic nanostructure are most determined by their size, shape, composition and structure. Hollow metallic nanostructures have attracted much interest as their surface plasmonic properties and catalytic activities are completely different from those of solid nanoparticles. Galvanic replacement reaction (GRR) was known to be a powerful synthetic technique for converting solid metal nanostructures into hallow ones. These hollow nanostructures have high specific surface area, low density, use less material and are cost effective. On the other hand, bimetallic-nanoparticles, in which two kinds of metals are contained in one particle, exhibit fascinating properties compared to those of the corresponding single-component particles. These particles are appeared to result from both the electronic and structural effects of the bimetallic structures. Nanoparticles fabricated from Ag-based alloys find extensive applications in catalysis, electro catalysis, and optics because their surface plasmon resonance (SPR) bands appear in the visible region.

It has been reported that the surface plasmon resonance peaks of hollow bimetallic Au/Ag nanostructures could be readily tuned by controlling the Ag-Au ratio of the replacement reaction. However, fewer attempts have been made to study the optical properties of Pt/Ag and Pd/Ag based bimetallic nanoparticles compared to those of the Ag-Au system, probably because Pt and Pd nanoparticles do not usually exhibit surface plasmon resonance peaks in the visible spectrum. However, it has been demonstrated recently that the surface plasmon resonance peak of Pd nanoparticles could be tuned to 520 nm by the formation of large hollow nanocages.

Hence, in this project, we have shown the efforts to come up with a new synthetic route for the controllable synthesis of Pt/Ag and Pd/Ag based bimetallic nanoparticles which exhibit tunable SPR extinction peaks in the visible region by applying galvanic replacement reaction on Ag templates in the presence of K_2PtCl_4 and K_2PdCl_4 salts. This report also focuses on the investigation of the characteristic optical properties of these composite hollow nanostructures.

Introduction

Noble metal-based bimetallic nanoparticles

Nanoparticles (NPs) have one or more dimensions in the nanometer scale (<100 nm) range and subsequently show novel properties from their bulk materials. Bimetallic composite nanoparticles, composed of two different metal elements, attract more attention than monometallic nanoparticles from both scientific and technological aspects due to potential unique electronic, optical, catalytic, or photocatalytic properties that are absent in the coincident monometallic nanoparticles. Nanoparticles composed of two different metal elements show better novel electronic, optical, and catalytic or photocatalytic properties compared to monometallic nanoparticles. Bimetallic nanoparticles could show not only the combination of the properties related to the presence of two individual metals, but also new properties due to a synergy between the two metals. The structure of bimetallic nanoparticles can be oriented in a random alloy, alloy with an intermetallic compound, a cluster-in-cluster, or core–shell structures and is strictly dependent on the relative strengths of metal-metalbonding, surface energies of bulk elements, relative atomic sizes, preparation method, and conditions.[1] Recent efforts have been devoted to metallic nanostructures, their fabrication, and applications as advanced materials

because of their intriguing chemical, electronic, optical, and catalytic properties.[2-5] Metallic nanostructure properties are determined by their shape, size, composition and structure.[6-12]

Optical Properties of monometallic and bimetallic noble metal nanoparticles

The color of colloidal dispersions of noble metal particles in fluid, typically water, varies from red to pink and from violet to blue for gold,[13] from yellow to orange, pink, and violet to grayish for silver,[14] from light brown to dark brown and black for platinum,[15] and dark brown for palladium,[16] depending upon the shape and size of the particles as well as the type of solvent. In case of bimetallic nanoparticles the color of colloidal dispersion is also dependent on the shape and size of nanoparticles, as well as the composition and metal distribution in bimetallic nanoparticles. The optical properties of noble metal particles originate from localized surface plasmon resonance (LSPR). Surface plasmon of a metal is a collective excitation of electrons in the conduction band and they dominate the electromagnetic responses of the metallic structure of dimensions on the order of the plasmon resonance wavelength. These phenomena happen when their electromagnetic fields interact with conduction band electrons which induces the coherent oscillation of electrons. As an effect, a strong absorption band appears in some region of the electromagnetic spectrum.[17]

When a conductor or metal is placed in an oscillating field of incoming radiation, the electron cloud is driven into an oscillation as shown in Figure 1. A complete theory of the scattering and absorption of electromagnetic radiation by a sphere, in order to understand the colors of colloidal gold particles in solution, was developed in 1908 by Mie.[18] The surface plasmonic properties and catalytic activities of hollow metallic nanostructures are completely different from those of solid nanoparticles. Hollow nanostructures also have lower density, high

specific area, use less material, and are lower in cost than solid nanoparticles.[19-20] Composite bimetallic nanoparticles, where two different kinds of metals are contained in one particle, exhibit properties that are very different from their single-component counter parts. These properties are assumed to be a result of the structural and electronic effects of the bimetallic structures.[21-22] Optical, electronic, and catalytic properties depend on the composition of the nanomaterials as well as their structure. The synthesis of bimetallic hollow nanostructures, as well as nanomaterials in general, has become a necessity for the future development of advanced nanotechnology. Acutely controlling the structures and compositions is crucial in order to obtain materials with specific properties. Previous experiments have reported that surface plasmon resonance peaks of hollow bimetallic Au/Ag nanostructures are able to be manipulated by controlling the Ag and Au ratio in the replacement reaction used.[23] There have however been fewer attempts in studying the optical properties of Pt or Pd based monometallic and bimetallic nanoparticles. One reason why there are fewer attempts is because Pt and Pd nanoparticles usually do not exhibit surface plasmon resonance peaks in the visible spectrum.[24] It has recently been shown that Pd surface plasmon resonance peaks can be tuned to 520 nm by forming large hollow nanocages.[25]

There has been an increased interest in nanostructures which are composed of metals in recent years because of the associated optical, electronics, optoelectronics, catalysis, sensing, clinical diagnostics, surface-enhanced Ramen scattering (SERS), information storage, and energy conversion/storage applications.[26] The performance of nanostructures can be improved by synthesizing them as hollow entities. Hollow nanostructures are advantageous due to a lower density coupled with a larger surface area. Nanoshells made from gold have been used to

expand the spectral range of surface plasmon resonance (SPR) which is associated with Au nanoshells.[27]

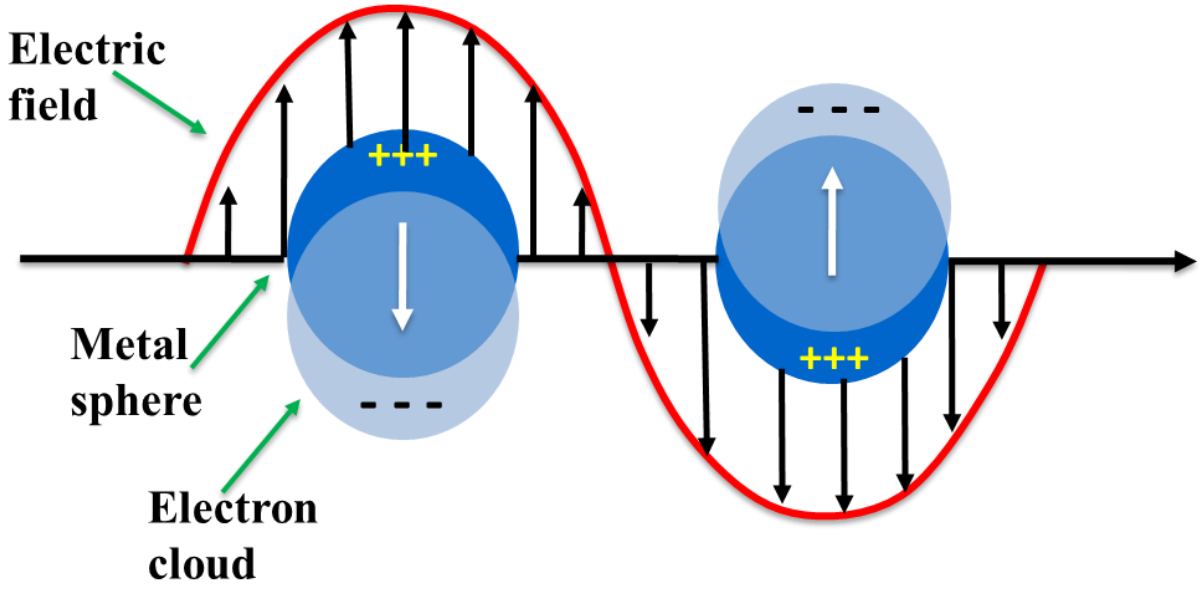

Figure 1. The electron cloud around the metal nanoparticles is excited by light photons. When the light hit the electron cloud, the cloud begins to oscillate resulting in polarization. The collective oscillation of the conduction electrons, in resonance with certain frequencies of incident light, leads to an excitation known as surface plasmon resonance (SPR).

Hollow metal nanostructures are prepared by templating against already existing entities like silica beads or polymer latexes. A thin shell of the desired metal is deposited on the surface of the template using various methods. The template can then be removed using wet chemical etching to create the hollow metal structure.[26] This process may seem simple but the resulting nanoshells often have problems such as incomplete coverage, poor crystallinity, nonuniformity in shell thickness, rough surfaces, structural fragility, as well as poorly controlled composition.

Galvanic Replacement Reaction

Among the strategies that have been reported to fabricate such unique hollow nanostructures galvanic replacement reactions offer a particularly effective, versatile, and robust approach for the generation of hollow nanostructures by replacing original metal or metal oxide sacrificial templates. These replacement reactions are driven by the redox potential difference of the two metal species. After the first report on the fabrication of Au hollow nanostructures from Ag NPs,[28] several research groups successfully extended the method to create other complex and multifunctional porous nanostructures and have thus explored their novel applications over the past decade.[29-32] For example, using morphology controlled Ag nanostructures as sacrificial templates a wide range of complex hollow nanostructures such as spherical nanoshells,[33] core−shell NPs,[34] nanodots,[35] nanocages,[36] nanotubes,[37] nanoframes,[38] and nanodendrites[39] composed of Au, Pd, and Pt. Multimetallic compositions have also been prepared via galvanic replacement synthesis reactions. Specifically, Xia and colleagues systematically uncovered the detailed mechanism of the galvanic replacement reaction between Ag NPs and $HAuCl_4$ in an aqueous solution.[40-41] Figure 2 Illustrates the galvanic replacement reaction converting solid metal nanostructures into hollow ones.

As shown in Figure 3, the replacement reaction includes two distinctive stages. At the initial stage the replacement reaction starts at specific sites with relatively high surface energies and then seamless hollow nanostructures, with smooth Au−Ag alloy walls, were evolved through an integration of galvanic replacement with alloying. Ag atoms also simultaneously migrate into the Au shell to form a seamless hollow nanostructure with an Au−Ag alloy wall. This mechanism for galvanic replacement is applicable irrespective of the morphology and

composition of the sacrificial templates it is, however, dependent on the presence of appropriate reduction potential differences between the two metals involved.

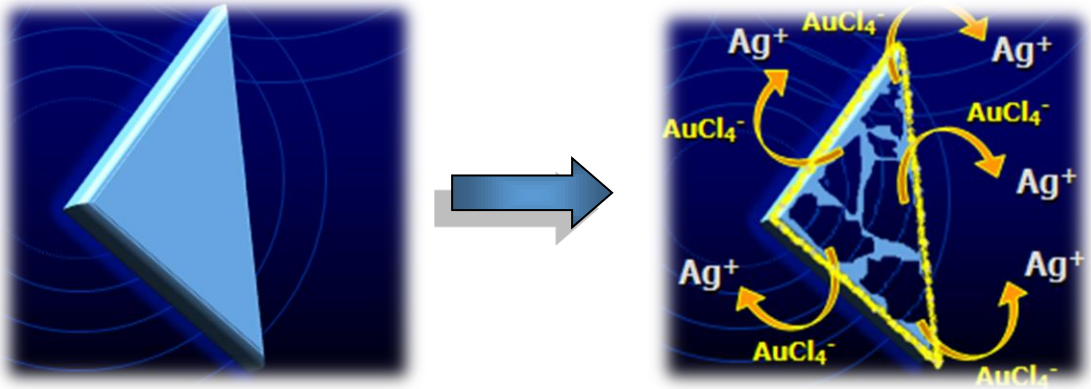

Figure 2. Schematic illustration of galvanic replacement reaction converting solid metal nanostructures into hollow ones. Due to the difference in electrode potentials one metal is used as a sacrificial template and it is reacted with ions of a more noble metal. The growth of the second metal takes place on the surface of the template to form a shell while the first metal is continuously consumed from the core.

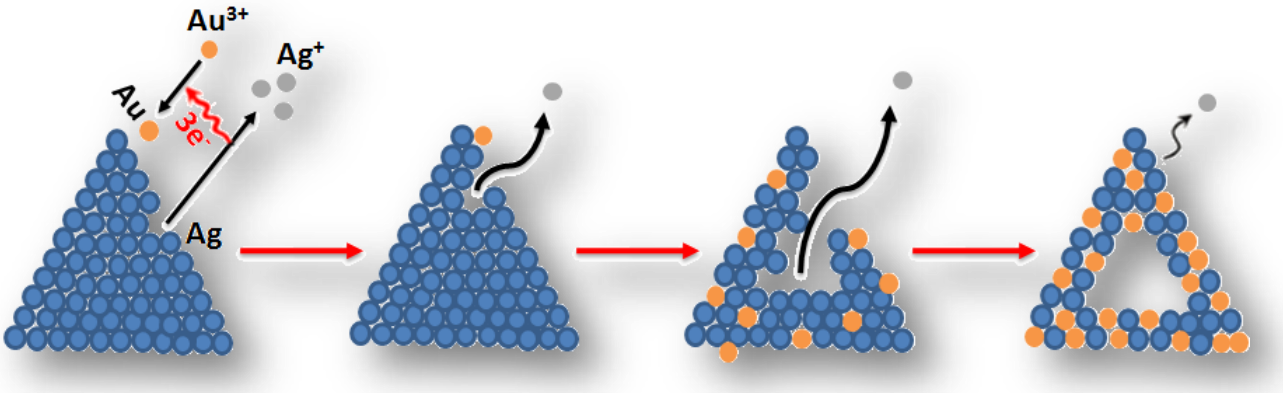

Figure 3. Schematic illustration of the morphological and structural evolutions at different stages of the galvanic replacement reaction between an Ag nanoprism and $HAuCl_4$ in an aqueous solution.

Experimental Section

Characterization

Spectroscopic Instrumentation and Methods. A PerkinElmer Lamda 35 UV-Vis spectrophotometer from Agilent Technologies was employed for absorption measurements as well as optical diffuse reflectance measurements. The absorption spectrum of the silver seed solution was measured, without dilution, while the silver nanoprism and Ag/Au hollow nanoprism solutions were diluted ×3 in Millipore water and their absorbance spectra obtained in the 1800 to 200 nm (0.68 eV ~ 6.2 eV) range.

Transmission Electron Microscopy (TEM) The TEM analysis was performed by using JOEL JEM-1230 analytical electron microscope with Gatanultrascan 4000 camera operating at a 120 kV acceleration voltage. One drop of the Ag/Au hollow nanoprism solution was added onto a carbon-coated copper TEM grid and the solvent was allowed to evaporate before introduction into the instrument.

Materials

Silver nitrate (99.9%) and sodium borohydride (98%) were purchased from Strem Chemicals. Poly(sodium-p-styrenesulfonate), citric acid, trisodium salt dihydrate (99%), L(+) ascorbic acid (99%), hydrogen tetrachloroaurate, potassium tetrachloroplatinate(II), and potassium tetrachloropalladate(II)were purchased from Acros.

Preparation of Ag Triangles of Different Sizes

The generatation of silver seeds requires aqueous trisodium citrate (5 mL, 2.5 mM), aqueous Poly(sodium-p-styrenesulfonate) (0.25 mL, 500 mg L^{-1}), and freshly prepared aqueous sodium borohydride (0.3 mL, 10 mM) which are combined in a 250 mL round bottom flask. Aqueous silver nitrate (5 mL, 0.5 mM) was added at a rate of 1 mL min^{-1} using a syringe pump while stirring the solution with a magnetic stir bar. The silver nanoprisms were created by combining Millipore water (5 mL), silver seed solution (20 µL,120 µL, 200 µL, and 650 µL), and aqueous ascorbic acid (75 µL, 10 mM), followed by the addition of aqueous silver nitrate (3 mL, 0.5 mM) at a rate of 1 mL min^{-1} using a syringe pump.

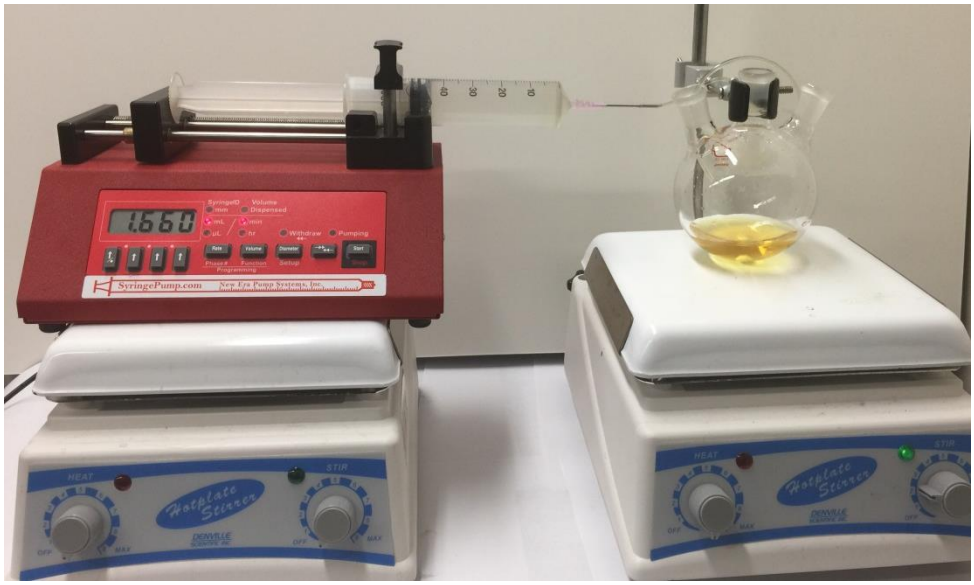

Figure 4. The programmable syringe pump used to gradually add small amounts of solution of $AgNO_3$ and $HAuCl_4$ at a given rate.

Synthesis of Ag/Au, Ag/Pd, and Ag/Ptalloy particles

The citrate capped Ag/Au, Ag/Pd, and Ag/Pt hollow nanoparticles were synthesized by following a literature method [28] with several modifications in order to prepare these particles on a larger scale. The synthesis of these nanoparticles begins with the synthesis of silver seeds which were then used to prepare silver nanoprisms. In the final step these nanoprisms were reacted with the gold, palladium, and platinum precursors.

The generation of silver seeds involved the addition of aqueous trisodium citrate (30 mL, 2.5 mM), aqueous Poly(sodium-p-styrenesulfonate) (1.5 mL, 500 mg L^{-1}), and freshly prepared aqueous sodium borohydride (1.8 mL, 10 mM) into a 250 mL round bottom flask. Aqueous silver nitrate (30 mL, 0.5 mM) was added to this three component solution at a rate of 1 mL min^{-1} using a syringe pump and stirring with a magnetic stir bar.

Silver nanoprisms were prepared by combining Millipore water (10 mL), silver seed solution (9.60 mL) and aqueous ascorbic acid (7.2mL, 10 mM), followed by the addition of aqueous silver nitrate (48 mL, 0.5 mM) at a rate of 1.66 mL min^{-1} using a syringe pump. After adding all of the silver nitrate the solution was vigorously stirred until the solution turned deep orange color permanently (usually this takes more than an hour).

Ag/Au, Ag/Pd, and Ag/Pt hollow nanoprisms were prepared by adding aqueous ascorbic acid (9mL, 10 mM) followed by $HAuCl_4$, K_2PdCl_4, or K_2PtCl_4 (60 mL, 0.5 mM) to the above prepared silver nanoprism solution at a rate of 1 mL min^{-1}.

Results and Discussion

Au/Ag alloy nanoshells were prepared by employing a galvanic displacement reaction of sacrificial Ag nanotriangles with $HAuCl_4$ as reported in the literature.[42] In addition, Pd/Ag spherical nanoshells and Pt/Ag triangular nanoshells were prepared by employing a similar synthesis method using K_2PdCl_4 and K_2PtCl_4, respectively, as metal precursors. The sacrificial Ag nanotriangles were produced by the reduction of $AgNO_3$ in the presence of PSSS using ascorbic acid as the reducing agent. Silver nanoprisms of varying size were created by adding different volumes of Silver seed solution (Table 1). Extinction spectra indicated that the surface plasmon resonance peak of the Ag nanoprism, which was prepared with decreasing amounts of silver seeds, red shifts compared to the SPR of pure Ag nanoparticles at 400 nm (Figure 5). Photographs of aqueous dispersions of the nanoparticles clearly show that the silver nanoprism revealed bright and distinctive colors as they were tuned across the visible spectrum (Figure 6). In other words the colors of the various solutions are dependent upon the absorption peaks at different wavelengths, based on the volume of silver seed added.

Table 1. Volumes of seed solution used to prepare silver nanoprisms of different sizes and their corresponding SPR peak position.

Ag Seed Solution Volume	SPR Peak position
20 µL	794 nm
120 µL	678 nm
200 µL	618 nm
650 µL	480 nm

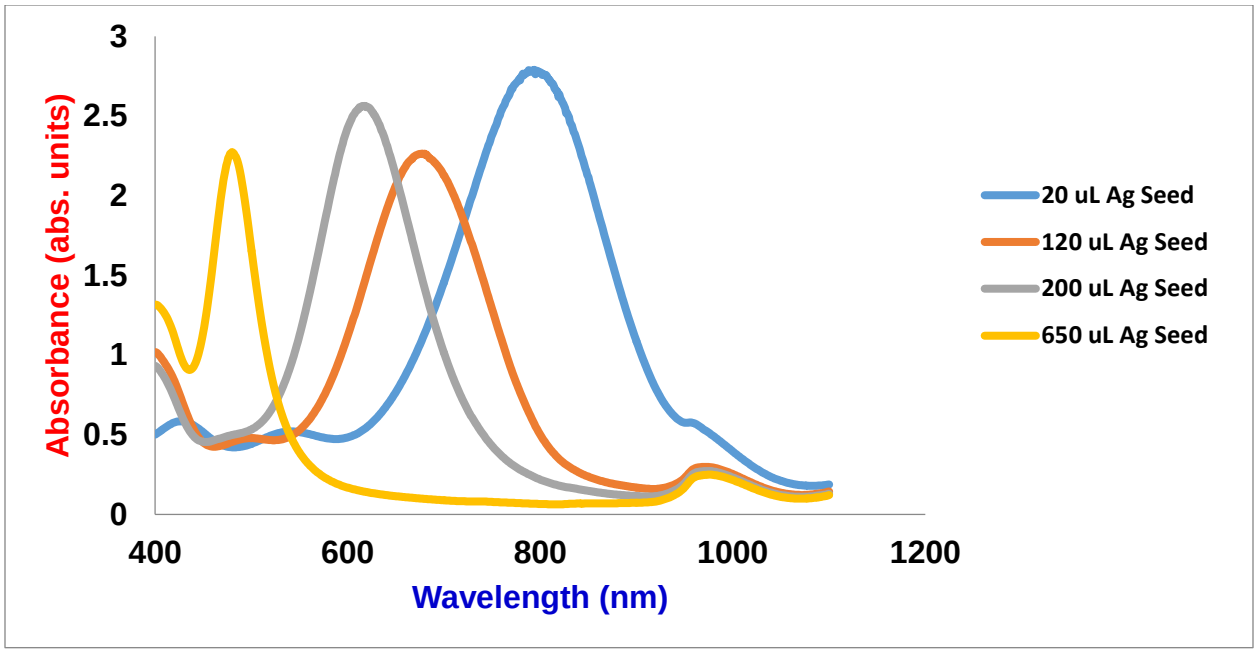

Figure 5. UV-Visible absorption spectra of the series of Ag nanoprisms obtained by using different volumes of seed solution:650 µL, 120 µL, 120 µL, and 20 µL.

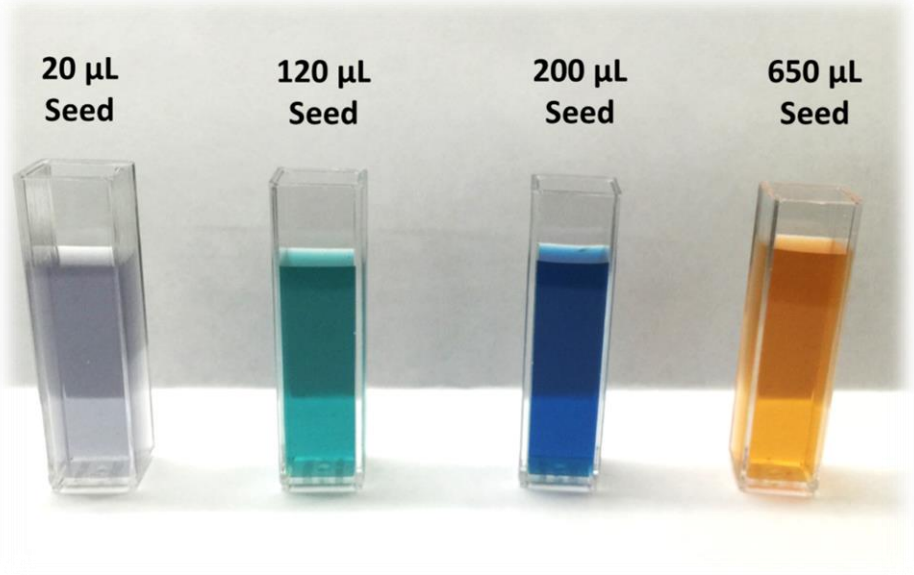

Figure 6. Photograph of the series of Ag nanoprism samples illustrating the range of colors obtained using different volumes of seed solution: 20 µL, 120 µL, 200 µL, and 650 µL.

Figure 7 shows UV-Visible absorption spectra for the series of Pd/Ag samples obtained by combining 40 μL, 80 μL, 120 μL, 160 μL, 200 μL, 240 μL, 280 μL, 320 μL, 360 μL, and 400 μL of K_2PdCl_4 (0.5 mM) with Ag nanoprisms in the presence of ascorbic acid using 120 μL of silver seed solution. The maximum absorbance peak for the Ag prism was 722 nm. The additional curves show the absorbance spectra of the Ag-Pd bimetallic particles with increased Pd composition. The surface plasmon resonance peaks of the particles with K_2PdCl_4 blue-shifted compared to the surface plasmon resonance of the pure Ag nanoparticle at 722 nm. As the volume of K_2PdCl_4continues to increase (120 μL and 400 μL), the surface plasmon resonance peaks continue to red-shift instead of blue-shift. The peaks continue to broaden and eventually diminish as can be seen with the addition of 400 μL of K_2PdCl_4. Figure 8 shows the photographs of aqueous dispersions of the Pd/Ag hollow particles which correspond to the UV-vis spectra (Ag prism and 400 μL Pd) in Figure 7. The evolution of the SPR is demonstrative of the changing structure of the nanoparticles during the reaction. This peak shift is hypothesized to be attributed to the increase in void size for composite bimetallic nanoshells and the formation of pinholes in the walls.[25]

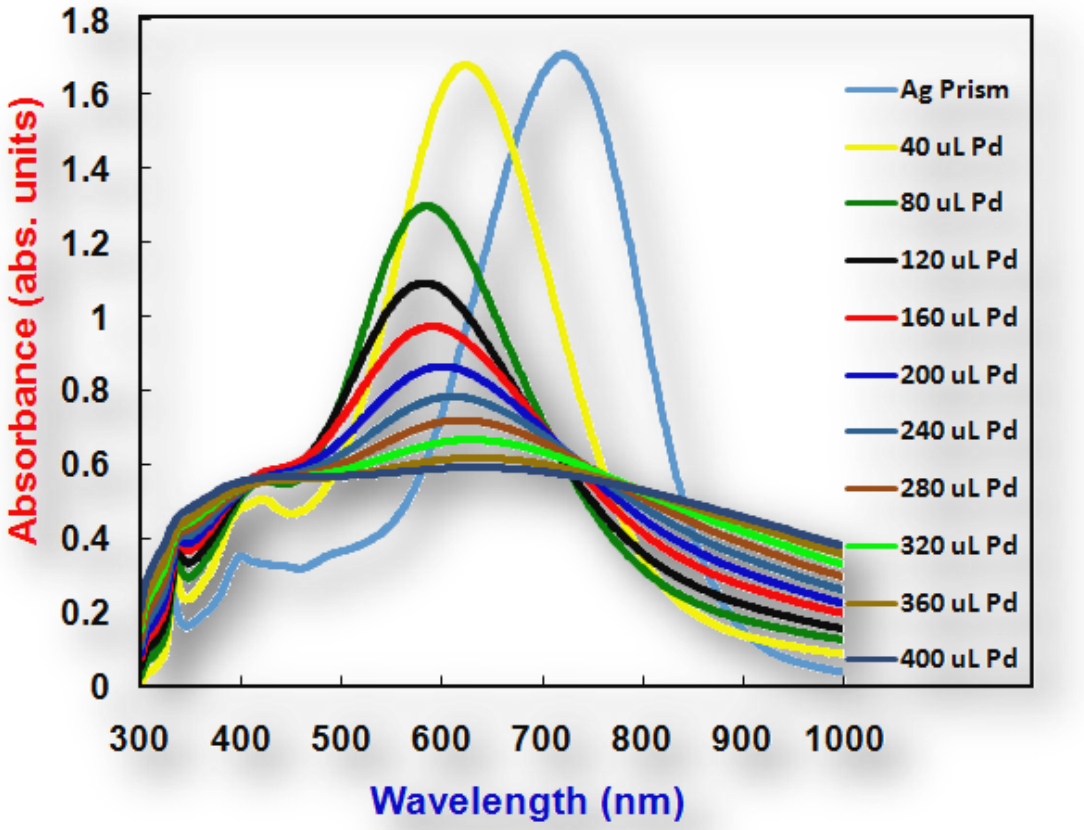

Figure 7. UV-Visible absorption spectra of the series of Pd/Ag samples obtained by addition of 40 μL, 80 μL, 120 μL, 160 μL, 200 μL, 240 μL, 280 μL, 320 μL, 360 μL, and 400 μL of K_2PdCl_4 (0.5 mM) in the presence of ascorbic acid to the Ag nanoprisms prepared by using of 120 μL of silver seed solution.

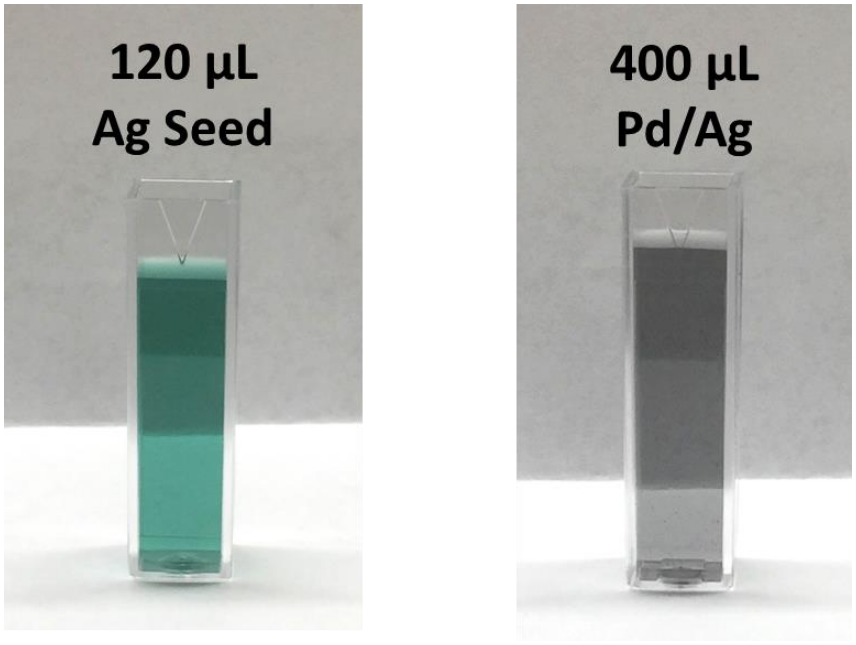

Figure 8. Photograph of Ag nanoprism solution obtained by using 120 µL of seed solution (left) and Pd/Ag samples obtained by addition of 400µL of K_2PdCl_4 solution (right).

Figure 9 shows UV-Visible absorption spectra of the series of Pt/Ag samples obtained by the addition of 40 µL, 80 µL, 120 µL, 160 µL, 200 µL, 240 µL, 280 µL, 320 µL, 360 µL, and 400 µL of K_2PtCl_4 (0.5 mM) in the presence of ascorbic acid to the Ag nanoprisms prepared by using 120 µL of silver seed solution. The maximum absorbance peak for the Ag Prism was 695 nm. The additional SPR peaks correspond to the Ag-Pt bimetallic particles with increased Pt content. The surface plasmon resonance peaks of the particles synthesized using the larger K_2PtCl_4 solution volumes lie at longer wavelengths and are further red-shifted in comparison with the surface plasmon resonance of the pure Ag nanoparticles at 695 nm. As the volume of K_2PtCl_4 continues to increase the surface plasmon resonance peaks continue to red-shift and broaden. Subsequent to the addition of 160 µL of K_2PtCl_4 the spectra significantly diminishes and continues to diminish until the addition of 400 µL of K_2PtCl_4. Figure 10 displays the photographs of the aqueous dispersions of Pt/Ag hollow nanoparticles which correspond to the

UV-vis spectra (Ag prism and 400 µL Pt) in Figure 9. The plasmonic properties of the bimetallic nanoparticles composed of Ag and Pt, which were prepared by successive reduction of $AgNO_3$ and H_2PtCl_6 by hydrazine, were reported by Gao et al.[43].The UV–Vis extinction peak along with the corresponding photograph of the colloids with different Pt content indicate that the surface plasmon resonance peak of the particles, which were prepared with higher content of H_2PtCl_6, red-shift further compared with the SPR of pure Ag and pure Pt nanoparticles at 430 nm. Photographs of the aqueous dispersions of the nanoparticles clearly show that the Ag–Pt nanoparticles revealed bright and distinctive colors as they were tuned across the visible light spectrum. When the amount of H_2PtCl_6 solution used during the preparation route surpassed a certain value the surface plasmon resonance peaks became broadened and blue shift rather than red shift before finally weakening. In our cases, the surface plasmon resonance peak of the Pt/Ag bimetallic particles red shifted when the volume of K_2PtCl_4 solution increased within a certain range (Figure. 9). This indicates that our present bimetallic system is similar the above-mentioned Pt/Ag alloy system and likely comprises nanostructures with hollow interiors as indicated from the microscopy results.

A substantial amount of material is needed for the property characterization to be carried out on a large scale synthesis; this was accomplished by scaling up the amounts of constituent compounds compared to the literature synthetic method[28] in order to synthesize larger Au/Ag, Pd/Ag, and Pt/Ag alloy samples. Because nanostructures made of gold and/or silver are known to exhibit distinctive SPR features that are strongly dependent on the composition, shape, and structure, the processes could also be conveniently observed using the UV-visible-NIR spectroscopic methods. Figure 11 shows UV-Visible absorption spectra, below is the series of Au/Ag samples obtained by the addition of 2 mL, 4 mL, 6 mL, 8 mL, 10 mL, 15 mL, 20 mL, 30

mL, 40 mL, 50 mL, and 60 mL of $HAuCl_4$ (0.5 mM), in the presence of ascorbic acid, to the Ag nanoprisms using 9.6 mL of silver seed solution.

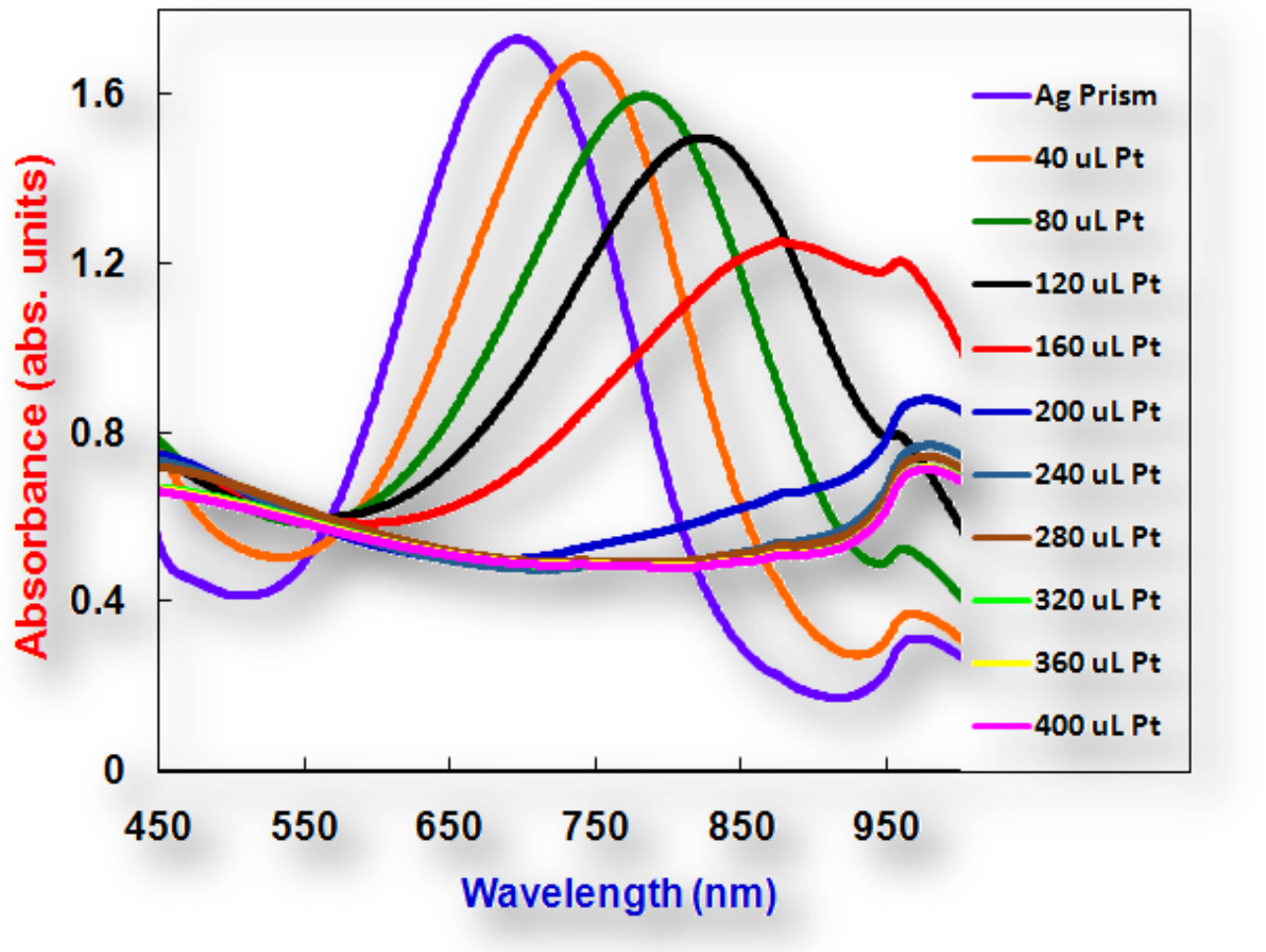

Figure 9. UV-Visible absorption spectra of the series of Pt/Ag samples obtained by addition of 40 µL, 80 µL, 120 µL, 160 µL, 200 µL, 240 µL, 280 µL, 320 µL, 360 µL, and 400 µL of K_2PdCl_4 (0.5 mM), in the presence of ascorbic acid, to the Ag nanoprisms prepared by using of 120 µL of silver seed solution .

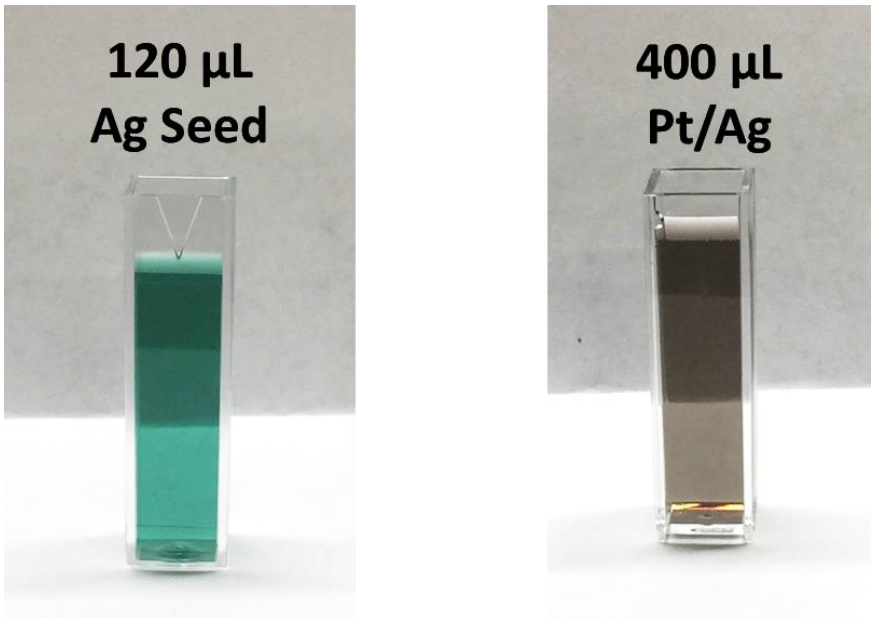

Figure 10. Photograph of Ag nanoprism solution obtained by using 120 µL of seed solution (left) and Pt/Ag samples obtained via the addition of 400µL of K_2PtCl_4 solution (right).

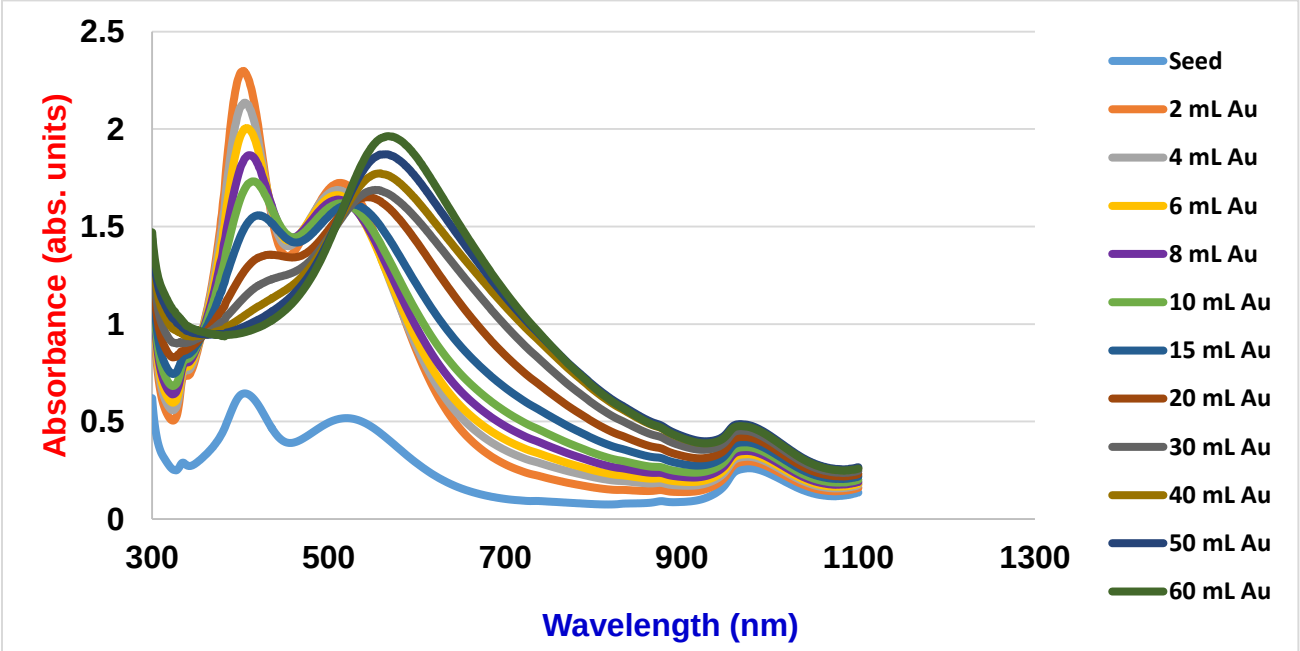

Figure 11. UV-Visible absorption spectra of the series of Au/Ag samples obtained by addition of 2 mL, 4 mL, 6 mL, 8 mL, 10 mL, 15 mL, 20 mL, 30 mL, 40 mL, 50 mL, and 60 mL of $HAuCl_4$ (0.5 mM), in the presence of ascorbic acid, to the Ag nanoprisms prepared by using of 9.5mL of silver seed solution.

The Ag nanoprism seed solution spectra was color-coded blue and the additional curves show the absorbance spectra of the Ag-Au bimetallic particles, with increased Au content for the large scale reaction. The surface plasmon resonance peaks of the particles with higher $HAuCl_4$ solution volumes lie at longer wavelengths and are red-shifted compared with the surface plasmon resonance of the pure Ag nanoprism seed solution. As the volume of $HAuCl_4$continues to increase the surface plasmon resonance peaks continue to red-shift and broaden. The absorbance which corresponds to the peak lies in the range of 370nm to 450 nm and increases initially when the addition of Au begins (2mL of $HAuCl_4$), but decline as more Au is added. Figure 11 shows the extinction spectra taken from a set of samples which were prepared by adding different volumes of a 0.5 mM $HAuCl_4$ solution to the Ag nanoprisms. More specifically, Figure 11 also shows the spectral changes involved in the formation of Au/Ag alloyed nanoshells. Note that the extinction peak corresponding to Ag nanoparticles (at 400 nm) disappeared when 40 mL of the $HAuCl_4$ solution was introduced into the reaction system. This change indicated the complete consumption of templates made of pure Ag as well as the formation of nanoshells composed of a homogeneous Au/Ag alloy. Accompanying the formation of Au/Ag nanoshells, an extinction peak with increasing intensity appeared at the longer wavelengths, and its position was continuously red-shifted toward 570 nm. This peak shift could be attributed to a slight increase in void size for the alloyed nanoshells.[44]

The UV-Visible absorption spectra shown in Figure 12 is from the series of Pd/Ag samples obtained by the addition of 10 mL, 20 mL, 30 mL, 40 mL, 50 mL, and 60 mL of K_2PdCl_4 (0.5 mM), in the presence of ascorbic acid, to the Ag nanoprisms which were prepared by using 9.5mL of of silver seed solution. The Ag nanoprism seed solution spectra is denoted in blue and the additional curves show the absorbance spectra of the Ag-Pd bimetallic particles with

increased Pd content for the large scale reaction. The surface plasmon resonance peaks of the particles with higher K_2PdCl_4 solution volumes lie at shorter wavelengths. Note that the extinction peak corresponding to Ag nanoparticles (at 577 nm) disappeared even when 10 mL of K_2PdCl_4 solution was introduced into the reaction system. As the volume of K_2PdCl_4continues to increase after addition of 10 mL the intensity of the surface plasmon resonance peaks continue to decrease and broaden. As the volume of K_2PdCl_4continues to increase (50mL-60mL) the surface plasmon resonance peaks continue to broaden until they diminish.

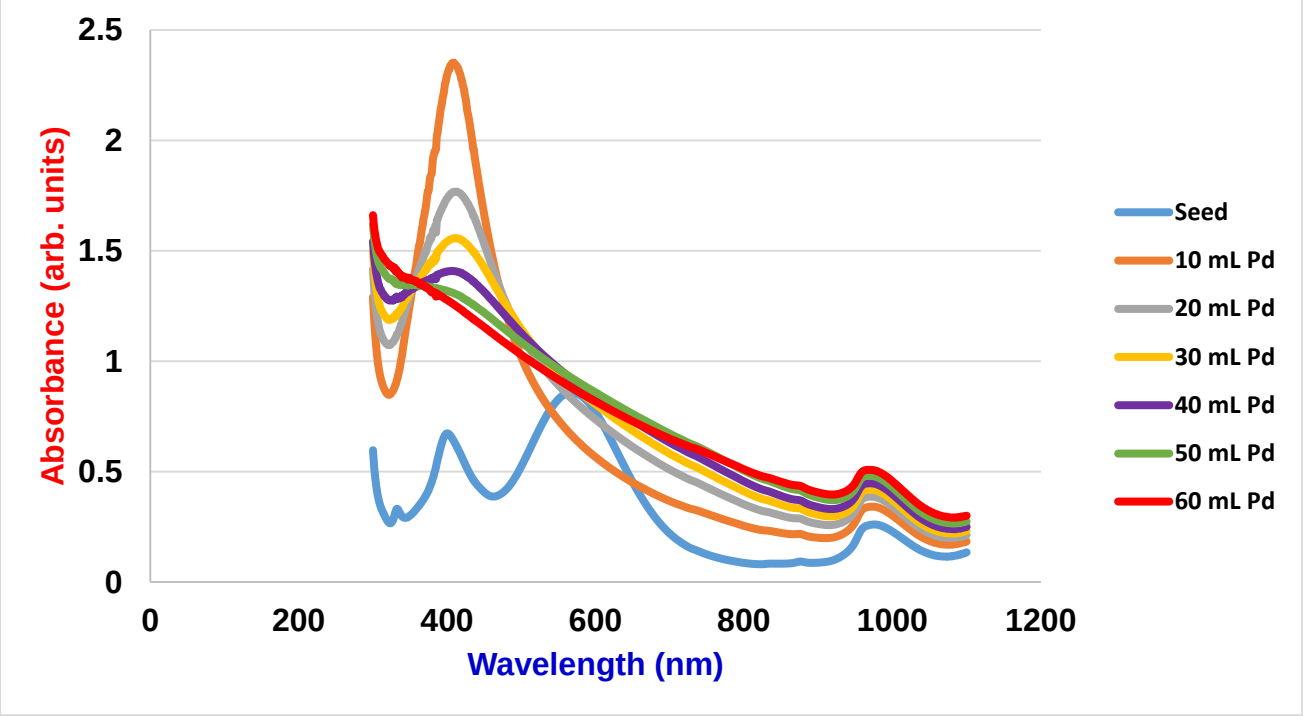

Figure12. UV-Visible absorption spectra of the series of Pd/Ag samples obtained by addition of 10 mL, 20 mL, 30 mL, 40 mL, 50 mL, and 60 mL of K_2PdCl_4 (0.5 mM), in the presence of ascorbic acid, to the Ag nanoprisms prepared by using of 9.5mL of silver seed solution.

UV-Visible absorption spectra shown in Figure 12 is from the series of Pt/Ag samples obtained by the addition of 2 mL, 4 mL, 6 mL, 8 mL, 10 mL, 20 mL, 30 mL, 40 mL, 50 mL, and 60 mL of K_2PtCl_4 (0.5 mM), in the presence of ascorbic acid, to the Ag nanoprisms prepared by using 9.5 mL of silver seed solution. The Ag nanoprism seed solution spectra is denoted in blue and the additional curves show the absorbance spectra of the Ag-Pt bimetallic particles with increased Pt content for the large scale reaction. The surface plasmon resonance peaks of the particles with higher K_2PtCl_4 solution volumes lie at longer wavelengths and are red-shifted compared with the surface plasmon resonance of the pure Ag nanoprism seed solution. As the volume of K_2PtCl_4continues to increase the surface plasmon resonance peaks continue to red-shift and broaden until they diminish.

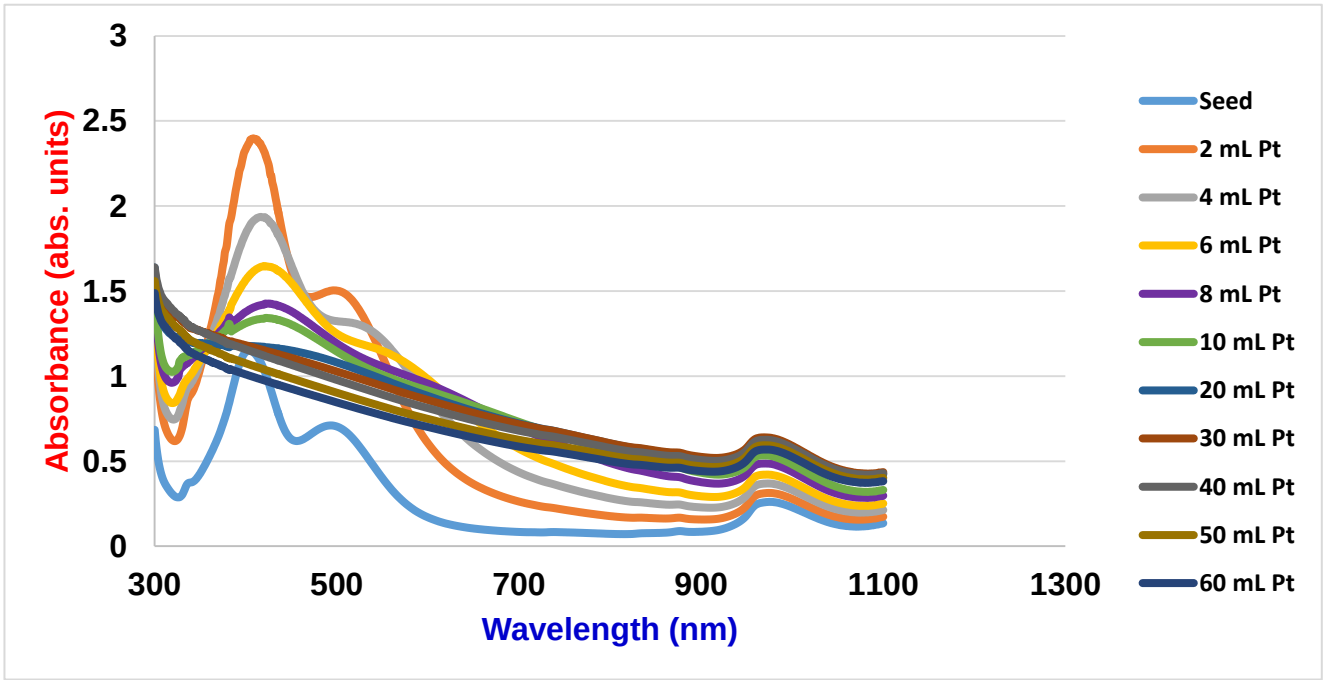

Figure13. UV-Visible absorption spectra of the series of Pt/Ag samples obtained by addition of 2 mL, 4 mL, 6 mL, 8 mL, 10 mL, 20 mL, 30 mL, 40 mL, 50 mL, and 60 mL of K_2PtCl_4 (0.5 mM), in the presence of ascorbic acid, to the Ag nanoprisms prepared by using 120 µL of silver seed solution.

Transmission scanning electron microscopy (TEM) was also employed to study the morphology of the Au/Ag, Pd/Ag, and Pt/Ag nanoshells. Transmission Electron Microscopy (TEM) is a technique that utilizes a beam of electrons that is transmitted through extremely small and thin specimens in a sample. The beam of electrons interacts with the specimens and an image is formed from that interaction. The TEM images shown in Figure 14 are of the individual (A) Au/Ag, (B) Pd/Ag, and (C) Pt/Ag nanoshells. The dark contrast areas in A and B represent the multilayers of nanoshells and illustrate the 3-dimensional connectivity of nanoscale. TEM images show that, in a majority of the individual Au/Ag alloy particles, small divided hollows have been created, whereas in Pd/Ag and Pt/Ag nanoshells, significantly larger single hollows (20−30 nm) have been created. Interestingly, in the case of Pt/Ag nanoshells narrowly dispersed triangular hollows were produced in a rapid manner.

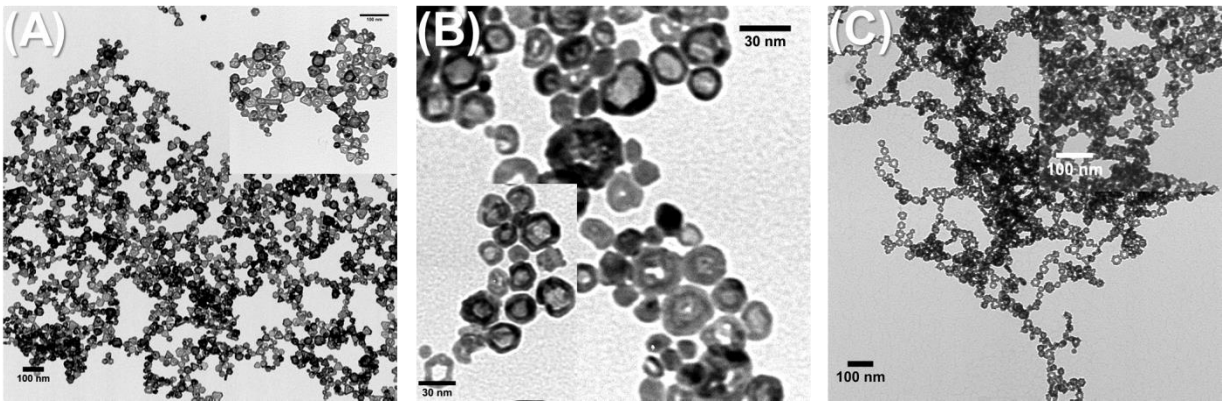

Figure14.TEM images of the individual (A) Au/Ag, (B) Pd/Ag, and (C) Pt/Ag nanoshells. The dark contrast areas in A and B represent the multilayers of nanoshells, illustrating the 3-dimensional connectivity of nanoscale.

Conclusion

In summary, Ag/Au, Ag/Pd, and Ag/Pt bimetallic hollow particles were successfully formed by employing a replacement reaction between Ag nanoparticles and aqueous $HAuCl_4$, K_2PdCl_4, and K_2PtCl_4using Ag nanoprism as sacrificial templates. These bimetallic nanostructures were intensively studied using UV-vis and TEM spectroscopy methods. We have presented here a simple method that exploit Ag template for the synthesis of Pd/Ag and Pt/Ag bimetallic hollow nanoparticles with a wide range of Pd and Pt content in order to tune the plasmon resonance peaks within the visible spectrum.

It has been demonstrated that the plasmon resonance peak locations, corresponding to these bimetallic hollow particles, could be tuned across the UV and visible spectrum by controlling the Pt and Pd content. This concept was reinforced by manipulating the composition, shape, and size of the noble metal nanoparticles and it has been shown that it is possible to design and construct nanostructures which can absorb photons of a desired wavelength.

References

1. Zaleska-Medynska, A.; Marchelek, M.; Diak, M.; Grabowska, E. *Adv. Colloid Interface Sci*. **2016**, *229*, 80–107.

2. Xia, Y.; Halas, N.J. *MRS Bull*. **2005**, *30*, 338-348.

3. Schulz, J.; Roucoux, A.; Patin, H. *Chem. Rev*. **2002**, *102*, 3757-3778.

4. Hu, M.; Chen, J.Y.; Li, Z.Y.; Au, L.; Hartland, G.V.; Li, X.D.; Marquez, M.; Xia, Y.N. *Chem. Soc. Rev*. **2006**, *35*, 1084-1094.

5. Graham, D.;Faulds, K.;Smith, W.E. *Chem. Commun*. **2006,** 4363-4371.

6. Jin, R.; Cao, Y.; Mirkin, C.A.; Kelly, K.L.; Schatz, G.C.; Zheng, J.G. *Science.***2001,** *294*, 1901-1903.

7. Burda, C.; Chen, X.; Narayanan, R.; El-Sayed, M.A. *Chem. Rev*. **2005,** *105*, 1025-1102.

8. Link, S.; Wang, Z.L.; El-Sayed, M.A. *J. Phys. Chem. B.***1999**, *103*, 3529-3533.

9. Kim, S.W.; Kim, M.; Lee, W.Y.; Hyeon, T.Y. *J. Am. Chem. Soc.***2002,** *124*, 7642-7643.

10. Kreibig, U.; Vollmer, M. *Optical Properties of Metal Clusters*; Springer: Berlin, 1995.

11. Sanedrin, R.G.; Georganopoulou, D.G.; Park, S.; Mirkin, C.A. *Adv. Mater*. **2005,** *17*, 1027-1031.

12. Rodriguez-Gonzalez, B.; Burrows, A.; Watanabe, M.; Kiely, C.J.; Liz Marzan, M. *J. Mater. Chem*. **2005,** *15*,1755-1759.

13. Pluchery O.; Remita H.; Schaming D. *Gold Bull.***2013**, *46*, 319–327.

14. Tan, Y.; Dai X.;, Li Y.; Zhu D. *J Mater Chem.***2003**,*13*, 1069–1075.

15. Yu, W.; Tu, W.; Liu, H. *Langmuir*. **1999**, *15*, 6–9.

16. Duteil, A.; Queau, R.; Chaudret, B.; Mazel, R.; Roucau, C.; Bradley. J. S. *Chem Mater.* **1993**, *5*, 341–347.

17. Mulvaney. P. *Langmuir*. **1996**, *12*, 788-800.

18. Mariscal, M.M.; Dassie, S. A. Leiva, E.P. *J Chem Phys.* **2005**, *123*, 184505:1–184505:6.

19. Sun, Y.; Xia, Y. *Anal. Chem*. **2002,** *74*, 5297-5305.

20. Liang, H.P.; Zhang, H.M.; Hu, J.S.; Guo, Y.G.; Wan, L.J.; Bai, C.L. *Angew. Chem. Int. Ed.* **2004,** *43*, 1540-1543.

21. Toshima, N.; Yonezawa, T. *New J. Chem*. **1998**, *11*, 1179-1201.

22. Sun, S.; Murray, C.B.; Weller, D.; Folks, L; Moser, A. *Science*. **2000,** *287*, 1989-1992.

23. Sun, Y.; Xia, Y.; *J. Am. Chem. Soc*. **2004**, *126*, 3892-3901.

24. Creighton, J.A.; Eadon, D.G. *J. Chem. Soc. Faraday Trans*. **1991,** *87*, 3881-3891.

25. Xiong, Y.; Wiley, B.; Chen, J.; Li, Z.; Yin, Y.; Xia, Y. *Angew. Chem. Int. Ed*. **2005,** *44*, 7913-7917.

26. Sun, Y.; Xia, Y. *Nano Letters*. **2003**, *3*, 1569-1572.

27. Oldenburg, S. J.; Averitt, R. D.; Westcott, S. L.; Halas, N. *J. Chem. Phys. Lett.***1998**, *288*, 243-247.

28. Sun, Y.; Mayers, B. T.; Xia, Y. *Nano Lett*. **2002**, *2*, 481−485.

29. Xia, X.; Wang, Y.; Ruditskiy, A.; Xia, Y. *Adv. Mater*. **2013**, *25*, 6313−6333.

30. Liu, Y.; Goebl, J.; Yin, Y.*Chem. Soc. Rev*. **2013**, *42*, 2610−2653.

31. Zhang, H.; Jin, M.; Liu, H.; Wang, J.; Kim, M. J.; Yang, D.; Xie, Z.; Liu, J.; Xia, Y. *ACS Nano*. **2011**, *5*, 8212−8222.

32. Alia, S. M.; Yan, Y. S.; Pivovar, B. S. **2014**, *4*, 3589−3600.

33. Gilroy, K. D.; Farzinpour, P.; Sundar, A.; Hughes, R. A.; Neretina, S. *Chem. Mater*. **2014**, *26*, 3340−3347.

34. Song, H. M.; Anjum, D. H.; Sougrat, R.; Hedhili, M. N.; Khashab, N. M. *J. Mater. Chem*. **2012**, *22*, 25003−25010.

35. Wang, C.; Wang, Y.; Xu, L.; Shi, X.; Li, X.; Xu, X.; Sun, H.; Yang, B.; Lin, Q. *A Small.* **2013**, *9*, 413−420.

36. Lu, X.; Au, L.; McLellan, J.; Li, Z.-Y.; Marquez, M.; Xia, Y. *Nano Lett*. **2007**, *7*, 1764−1769.

37. Chen, Z.; Waje, M.; Li, W.; Yan, Y.*Angew. Chem., Int. Ed*. **2007**, *46*, 4060−4063.

38. Wan, D.; Xia, X.; Wang, Y.; Xia, Y. *Small*.**2013**, *9*, 3111−3117.

39. Zhang, G.; Sun, S.; Cai, M.; Zhang, Y.; Li, R.; Sun, X. *Sci. Rep*. **2013**, *3*, 1526-1554.

40. Sun, Y.; Xia, Y. *J. Am. Chem. Soc*. **2004**, *126*, 3892−3901.

41. Sun, Y. G.; Xia, Y. N. *Nano Lett*. **2003**, *3*, 1569−1572.

42. Aherne, D.; Gara, M.; Kelly, J. M.; Gun'ko, Y. K. *Adv. Funct. Mater*. **2010**, *20*, 1329-1338.

43. Gao J, Ren X, Chen D, Tang F, Ren J. *Scr Mater*. **2007**, *57*, 687–690.

44. Westcott, S. L.; Oldenburg, S. J.; Lee, T. R.; Halas, N. J. *Chem. Phys. Lett*. **1999**, *300*, 651-655.